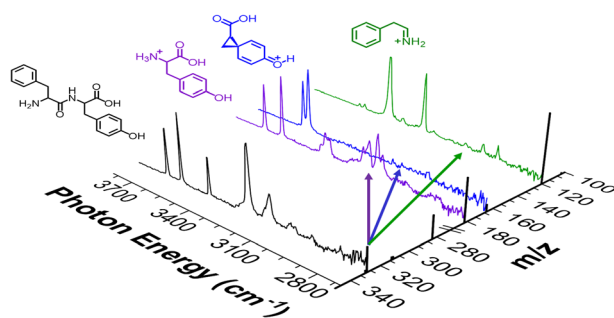Check for updates

**RESEARCH ARTICLE**

# Integration of High-Resolution Mass Spectrometry with Cryogenic Ion Vibrational Spectroscopy

Fabian S. Menges, Evan H. Perez, Sean C. Edington, Chinh H. Duong, Nan Yang, Mark A. Johnson [ORCID]

Department of Chemistry, Yale University, New Haven, CT 06520, USA

**Abstract.** We describe an instrumental configuration for the structural characterization of fragment ions generated by collisional dissociation of peptide ions in the typical MS$^2$ scheme widely used for peptide sequencing. Structures are determined by comparing the vibrational band patterns displayed by cryogenically cooled ions with calculated spectra for candidate structural isomers. These spectra were obtained in a linear action mode by photodissociation of weakly bound $D_2$ molecules. This is accomplished by interfacing a Thermo Fisher Scientific Orbitrap Velos Pro to a cryogenic, triple focusing time-of-flight photofragmentation mass spectrometer (the Yale TOF spectrometer). The interface involves replacement of the Orbitrap's higher-energy collisional dissociation cell with a voltage-gated aperture that maintains the commercial instrument's standard capabilities while enabling bidirectional transfer of ions between the high-resolution FT analyzer and external ion sources. The performance of this hybrid instrument is demonstrated by its application to the $a_1$, $y_1$ and $z_1$ fragment ions generated by CID of a prototypical dipeptide precursor, protonated L-phenylalanyl-L-tyrosine (H$^+$-Phe-Tyr-OH or FY-H$^+$). The structure of the unusual $z_1$ ion, nominally formed after NH$_3$ is ejected from the protonated tyrosine ($y_1$) product, is identified as the cyclopropane-based product is tentatively identified as a cyclopropane-based product.

**Keywords:** Cryogenic vibrational spectroscopy, MS$^2$, Peptide ion fragment structure, Orbitrap, High-resolution mass spectrometry

## Introduction

Structural characterization of mass-selected ions with infrared (IR) vibrational spectroscopy is an increasingly valuable secondary analysis tool for mass spectrometry [1–6]. This technique is most powerful when carried out with cryogenically cooled ions, either in a mass messenger or "tagging" mode [1, 7–9] or in a tag-free approach based on two color, IR-IR or IR-ultraviolet/visible double-resonance excitation [10, 11]. In that scheme, the spectra are obtained for ions frozen close to their global (or sometimes local) minima in a linear action mode such that they can be directly compared with the patterns calculated for candidate structures using increasingly sophisticated electronic structure software packages (e.g., Gaussian, GAMESS, Turbomole, and Schrödinger) [1, 3–5]. Ions are typically cooled with a buffer gas in a cryogenic (~ 4 K) radio frequency (RF) ion trap [12–21], and IR spectra are obtained by photodissociation in a tandem mass spectrometry (MS) mode. Specific implementations range from double focusing time-of-flight (TOF) [22–24] to photoexcitation in mass-selective traps followed by mass analysis. Secondary mass analysis can then be carried out with a variety of techniques such as time-of-flight, mass selection with a quadrupole mass filter, and multiplexing Fourier transform (FT) schemes based on electrostatic (Orbitrap) [25, 26] or magnetic (ion cyclotron resonance (ICR)) [27] ion traps. Many of these hybrid instruments are

---

*Correspondence to:* Mark Johnson; *e-mail:* mark.johnson@yale.edu

based on customized commercial platforms and retain their original ion processing capabilities. As such, characterization of ion structures with cold ion spectroscopy brings a powerful addition to the arsenal of secondary analysis methods already integrated into these instruments. Here, we describe our integration of cryogenic vibrational spectroscopy into the Thermo Fisher Orbitrap Velos Pro (hereafter denoted "Velos") in an arrangement where ions processed using its secondary analysis capabilities are structurally characterized by analyzing their vibrational spectra. We demonstrate the performance of this hybrid platform by applying it to several fragment ions generated by collision-induced dissociation (CID) using MS/MS ($MS^2$) analysis of a prototypical dipeptide cation.

We focus on the structural identification of CID fragment ions because this method is widely available in commercial instruments and provides a powerful means for characterization of complex chemical samples. Particularly important applications in this regard are proteomics [28], de novo sequencing [29], and metabolite analysis [30]. Peptide analysis typically relies on previous knowledge of the fragmentation pathways to identify cleavage points. The resulting CID fragments are then cataloged by the formation of $a_x$, $b_x$, and $y_x$ ions [29] which often involve chemical rearrangements (e.g., proton migration). The utility of vibrational spectroscopy in analyzing the mechanisms that drive fragmentation has recently been demonstrated in an arrangement where infrared multiphoton dissociation (IRMPD) spectra of room temperature ions were obtained using a modified Bruker Paul trap [31]. In that case, the structures of the fragment ions generated by electron-transfer dissociation (ETD) from a five-residue polypeptide ($[AAHAR+2H]^{2+}$) were established by comparison with calculated band patterns at the harmonic level for candidate structures [28, 32].

Although it represents a significant advance, the IRMPD approach [33] suffers from the important complication that the resulting spectra reflect highly non-linear (> 15 photons) excitation processes and are obtained with (~ 300 K) ions whose internal energies are far above their global minima. Here, we address this limitation by integrating a cryogenic ion vibrational spectroscopy instrument with a commercial, high-resolution tandem mass spectrometer. We demonstrate the hybrid instrument's performance through the structural characterization of fragment ions generated by the routine $MS^2$ operation of the Velos. For this purpose, we focus on a simple dipeptide (protonated L-phenylalanyl-L-tyrosine, abbreviated hereafter as FY-$H^+$). Using CID is carried out in the linear quadrupole trap (LTQ) section of the instrument to obtain the fragmentation pattern, as is usual in the course of sequencing by $MS^2$. The fragment ions are first analyzed using the high-resolution Orbitrap capability of the instrument then passed onto the cryogenic ion spectrometer for further characterization by IR action spectroscopy. In this way, we effectively realize an "add-on" analysis tool that fully maintains the inherent functionality of the commercial instrument; the hybrid instrument makes possible the structural characterization of $MS^n$ products or intermediates extracted directly from the fragmentation cell while leaving the essential capabilities of the commercial device intact.

## Overview of the Instrument

Figure 1 presents a schematic diagram of the Yale hybrid instrument. The interface was achieved by replacing the Orbitrap's C-trap exit aperture and subsequent higher-energy collisional dissociation (HCD) trap with a custom C-trap interface aperture (CTIA) and octopole ion guide to lead ions out of the commercial instrument and into the Yale triple-focusing photofragmentation mass spectrometer (see photographs in Fig. S1) [11]. We implement external control of the CTIA to gate the flow of ions according to several protocols. The timing of the external components is slaved to the aperture control generated by the Velos software (see triggering scheme in Fig. S2). The external control of the CTIA to a repelling mode was optimized to maintain the high-resolution performance of the Orbitrap mass analyzer (see comparison in Fig. S3). In this way, routine $MS^n$ measurements can be carried out on target ions with both LTQ and FT modes to allow traditional structural analysis. When one is interested in further characterizing an ion using cryogenic vibrational spectroscopy, however, an ion packet created in the LTQ part of the instrument is launched toward the C-trap with its trapping buffer gas turned off. Lowering the direct current (DC) voltage on the CTIA then allows the ion packet to pass through the C-trap to the octopole guides leading them out of the instrument and into the Yale spectrometer. In the current configuration, the drift path length between the two instruments is about 1.5 m due to the physical dimensions of the two. The transition section includes several control apertures and a gate valve [34] to enable isolation of the Orbitrap and Yale TOF vacuum envelopes, as well as a bent octopole ion guide to match the angles of the two instruments.

The pulse cycle of the Yale spectrometer is triggered by the Velos timing pulse (conveniently intercepted at BNC connector J6722 on the RF control board) linked to the injection of C-trap ions into the Orbitrap (see timing sequence in Fig. S2). This serves to synchronize the ion packet leaving the LTQ component of the Velos with the pulsed valve that introduces buffer gas into the cryogenically cooled Paul trap at the start of the Yale triple-TOF photofragmentation spectrometer. The (~ 1 ms) buffer gas pulse is introduced about 20 ms before the arrival of the LTQ ion packet. The buffer gas mixture (10% $D_2$ in He) is optimized to enable attachment of weakly bound adducts to the ions of interest. The vibrational predissociation spectra of these "tagged" ions are then obtained with the TOF-based, triple-focusing photofragmentation mass spectrometer described previously [11]. Technical details of the interface are included in the supplementary materials (Section 1). We note that the Yale spectrometer includes its own electrospray ionization source, and the ion transfer facility of the hybrid instrument is bidirectional. Thus, it is also possible to perform high-resolution (Orbitrap) mass spectrometry on the ions generated using the Yale electrospray source. A comparison of the peak shapes generated by the Orbitrap analyzer at maximum resolution (100,000 Δm/m at 200 *m/z*) for various configurations is presented in Fig. S3. This dual-use capability is achieved by introducing the Velos ions to the Yale TOF with a DC 90°
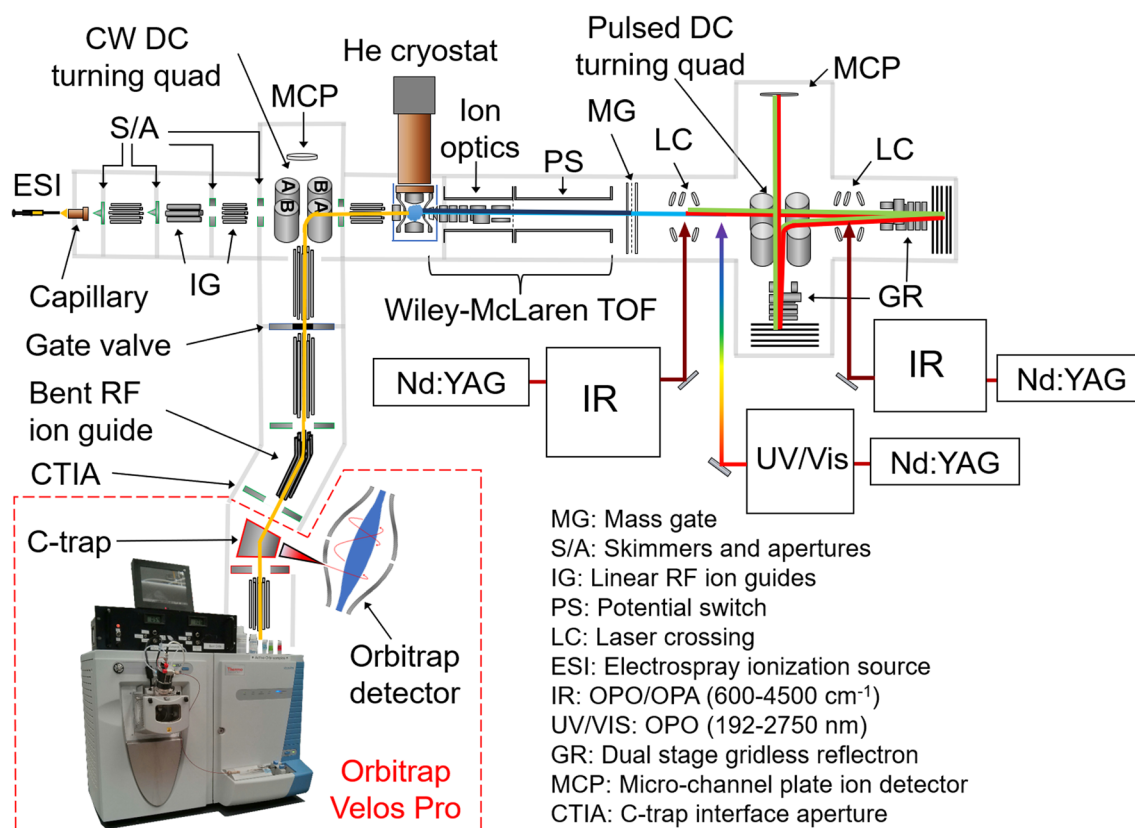
**Figure 1.** Scheme of the hybrid instrument that integrates a high-resolution Thermo Fisher Scientific Orbitrap Velos mass spectrometer with a custom-built cryogenic, triple-focusing photofragmentation mass spectrometer. Components of the commercial Velos Pro are grouped inside the red dashed lines and include a commercial Thermo Fisher ESI source and LTQ ion trap, which are both part of the embedded photograph but not explicitly shown. The external ESI and linear ion guides provide an independent ion source for species not readily prepared in the commercial instrument (e.g., $M^+(H_2O)_n$)
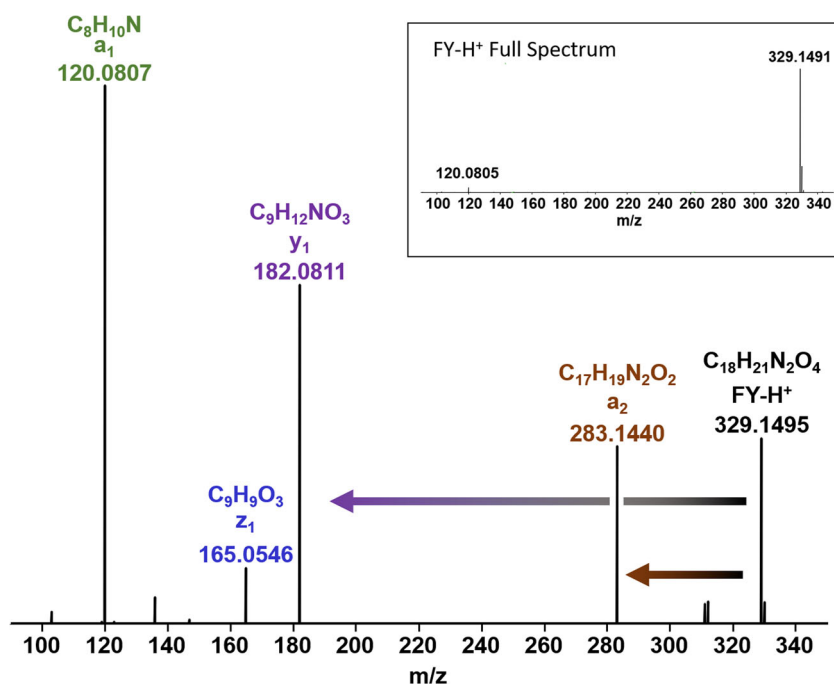


**Figure 2.** CID mass spectrum of the FY-$H^+$ parent ion (329 $m/z$, black) displaying four major fragmentation pathways: $a_1$ (120 $m/z$, green), $y_1$ (182 $m/z$, purple), $a_2$ (283 $m/z$, brown), and a weak $z_1$ product (165 $m/z$, blue). Molecular compositions were generated using the ThermoQual software. See Table S1 for simulated masses and deviations

turning quadrupole (see schematic in Figure 1). In this way, setting the turning quadrupole to transmission mode enables spectroscopic interrogation of ions from the Yale source in the mode utilized for many previous studies [1].

## Cryogenic Vibrational Spectra of MS$^2$ Fragments and Comparison with Harmonic Calculations of Candidate Structures

FY-H$^+$ was isolated and fragmented in the LTQ section of the Orbitrap Velos Pro with normalized collision energy (NCE) of 29 and 10 ms activation time. The resulting CID fragment ions were transferred into the cryogenic Paul trap for cooling and D$_2$ tagging. The ions were then mass-separated using the Yale TOF photofragmentation spectrometer. Additional sample preparation details are included in the SI.

A typical FY-H$^+$ fragmentation mass spectrum is shown in Figure 2 alongside molecular composition assignments of

the fragmentation products derived from common fragmentation pathways (a$_1$, y$_1$, a$_2$) [28]. After the masses of the parent and fragment ions were confirmed using the high-resolution capability of the Orbitrap, they were sent on to the Yale TOF spectrometer for structural analysis with cryogenic vibrational spectroscopy. Scans of the vibrational spectra were acquired in two different spectral regions (900–2000 cm$^{-1}$ and 2800–3800 cm$^{-1}$), with each scan taking 15 min. Overall signal-to-noise was improved by averaging over many individual scans. Depending on the ion abundance, the acquisition times for the results presented in Figure 3 ranged from 2 h for the most abundant ion (FY-H$^+$) to 8 h for the least abundant ion (the z$_1$ fragment). The structures of most of the fragments are anticipated based on precedent: the a$_1$ ion likely occurs via formation of the iminium ion, the a$_2$ ion can be generated by the loss of neutral formic acid, and the y$_1$ fragment presumably forms after cleavage of the amide bond.

The D$_2$-tagged spectra of the FY-H$^+$, a$_1$, and y$_1$ ions are shown in Figure 3. Each displays a series of sharp peaks throughout the range 900–4000 cm$^{-1}$. Density functional
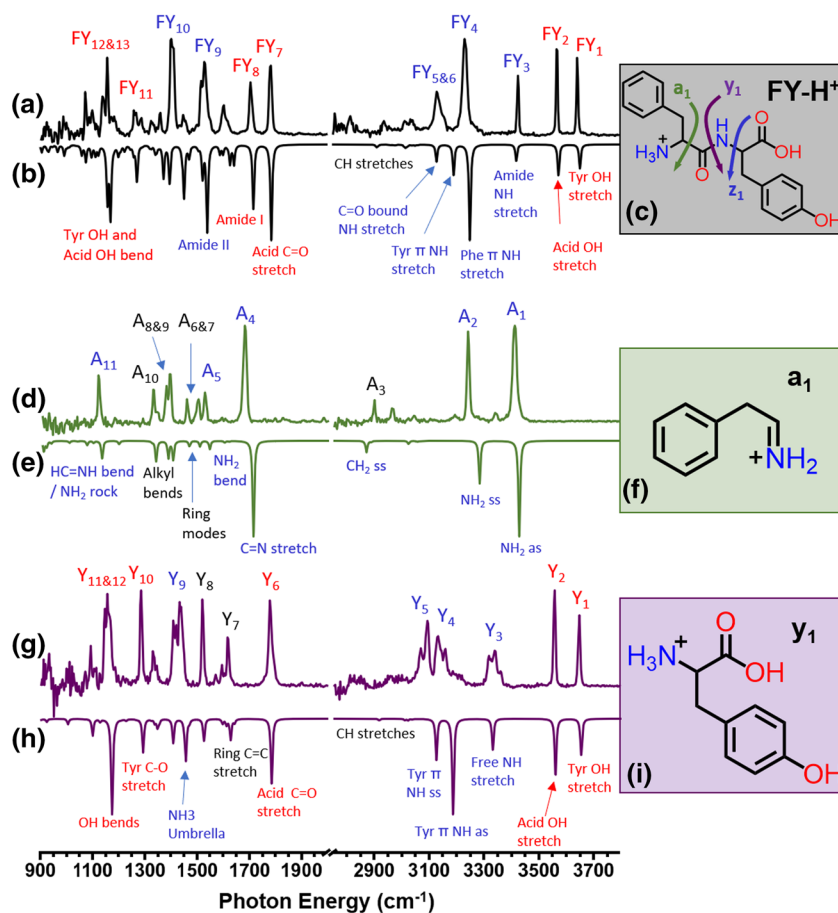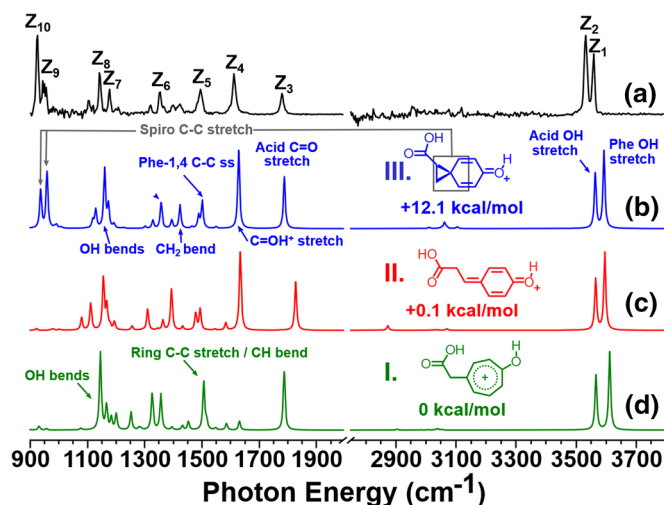


**Figure 3.** Photofragmentation spectra of the D$_2$-tagged FY-H$^+$ parent (**a**), a$_1$ (**d**), and y$_1$ (**g**) fragments. Calculated spectra, derived from electronic structure calculations of the fragments' structural minima, are inverted underneath the corresponding spectra in (**b**), (**e**), and (**h**) demonstrating good agreement between experiment and theory. Chemical structures for each species are shown in (**c**), (**f**), and (**i**). Labeled peaks in (**a**), (**d**), and (**g**) can be found in Table S2. Labels for assignments are colored black for CC and CH modes, blue for N modes, and red for O modes

theory (DFT) calculations (B3LYP/6-311G++(d,p)) using Gaussian 09 [35] converged on structures that are consistent with those expected for the FY-H$^+$ and $a_1$ ions, while the $y_1$ spectrum is very similar to that reported in detail for protonated tyrosine [36]. The multiplet structure in the $y_1$ spectrum ($Y_3$, $Y_4$, and $Y_5$) indicates that this ion occurs in several different conformers upon cooling that have been spectroscopically isolated using IR/UV double-resonance methods [36]. The FY-H$^+$ and $a_1$ structures at the right of Figure 3 were the lowest in energy among other locally stable minima. The identification of the $y_1$ fragment ion as protonated tyrosine through its characteristic cryogenic vibrational spectrum highlights one of the powerful features of this method. Specifically, this is possible because the spectrum is obtained using linear action and applies to the vibrationally cold ions. As such, these spectra are directly comparable with those reported earlier even though the ions may have been prepared under very different conditions. Consequently, a library of such spectra [37, 38] would create a more accurate fingerprint of the molecular structures because they are not subject to variations that are intrinsic to the MS$^2$ approach. These variations include different protocols for pressure, collision gas, and collision energy, as well as whether dissociation is carried out under single or multiple collision regimes [39, 40].

The predicted (scaled, see SI for scaling protocols) harmonic spectra for these structures are presented as the inverted traces in Figure 3. The vast majority of the observed transitions are indeed recovered at the simple harmonic level with remarkably similar intensity profiles. This agreement provides detailed structural identifications of the fragments that are indeed consistent with accepted fragmentation patterns. For example, protonated tyrosine (the $y_1$ fragment) is nominally formed by cleavage of the amide bond (purple arrow in Figure 3c) and thus retains the OH stretches ($Y_1$ and $Y_2$) that are present in the FY-H$^+$ spectrum (FY$_1$ and FY$_2$). Similarly, both FY-H$^+$ and $y_1$

spectra contain features arising from their other shared structural motifs, such as the acid C–O stretches (FY$_7$ and Y$_6$), O–H bends (FY$_{12\&13}$, Y$_{11\&12}$), and tyrosine C–OH stretch (FY$_{11}$, Y$_{10}$). Furthermore, comparison of the observed and calculated spectra of FY-H$^+$ allows us to establish that protonation occurs at the N terminus. The NH groups of this –NH$_3^+$ moiety form linkages with the amide C=O group and the $\pi$ clouds of the tyrosine and phenylalanine side chains. The NH stretches account for bands (FY$_4$, FY$_5$, Y$_4$, Y$_5$), which occur ~80 cm$^{-1}$ below those found in an isolated –NH$_3^+$ motif [23]. On the other hand, the $a_1$ fragment [41] is generated by breakup at the green arrow in Figure 3c (with proton migration), leading to a new strong band (A$_4$) arising from the C=N stretch in the iminium functionality with the higher energy doublet (A$_1$ and A$_2$) derived from the symmetric and asymmetric stretches of the NH$_2$ group. Note that these bands are also red-shifted (~ 40 cm$^{-1}$ and 100 cm$^{-1}$ for the asymmetric and symmetric stretches, respectively) relative to their calculated positions in the higher energy rotamer where the phenyl group is displaced away from the NH$_2$ motif (Figs. S4–S6).

The weak $z_1$ fragment is interesting in that it corresponds to the mass expected for heterolytic cleavage at the strong C$_\alpha$–N bond (blue arrow in Figure 3c), which is an unusual pathway for CID of protonated peptides [42]. This yields a closed shell carbocation with several chemically distinct rearrangement pathways, for which there is no strong precedent upon which to formulate a structural hypothesis. It is clear from the D$_2$-tagged spectrum (Figure 4a), however, that the observed fragment features two free OH groups (Z$_1$ and Z$_2$) and retains the acid C=O (Z$_3$). We therefore carried out an extensive search for possible structures that retain these functionalities, starting from different initial conformations and applying geometric constraints to either promote or prevent chemical rearrangements such as ring formation. Details about the constraints are included in the SI (section 2). Three low-lying structural



**Figure 4.** Photofragmentation spectrum of the $z_1$ fragment (**a**) and calculated spectra corresponding to candidate structures involving formation of a cyclopropane-containing spiro compound (**b**), proton migration (**c**), and formation of a hydroxytropylium cation (**d**). Calculated spectra are derived from DFT calculations of the species' structural minima. Labeled peaks in (**a**) can be found in Table S3

isomers were identified (hereafter denoted isomers I, II, and III) that are indicated in the inserts in Figure 4 with rotating pdf images in Figs. S9–S11. These isomers differ in the structure of the hydrocarbon backbone, with the lowest energy isomer (I) based on a hydroxytropylium scaffold, while the two higher energy isomers feature a 1,4-cyclohexadiene hydrocarbon core. The strong $Z_4$ feature is not present in the predicted spectrum of I, but is recovered in the harmonic prediction for the two higher energy isomers as due primarily to the CO displacement in the $C=OH^+$ functionality. Finally, the telltale ($Z_9$ and $Z_{10}$) bands, which dominate the low-energy region of the observed spectrum, are only present in the highest energy isomer (III). In fact, the overall agreement with the observed spectrum is compelling for the assignment of the observed fragment to this interesting spiro-bicyclic scaffold with a cyclopropane motif. Further investigation of this species is clearly warranted to verify this hypothesis, and if confirmed to explore the pathways for isomer interconversion. This observation highlights how cryogenic spectroscopy can reveal unexpected chemical rearrangements in minor species present in CID analysis but not generally utilized for sequencing.

## Conclusion and Outlook

We described the design, operation, and demonstration of a hybrid instrument that combines a commercial high-resolution mass spectrometer with a custom-built, cryogenic ion photofragmentation infrared spectrometer. This scheme adds bond-specific structural information to the $MS^n$ scheme widely used for compound identification. The vibrational predissociation spectra of the ~20-K fragment ions formed by CID in the LTQ trap of a commercial Thermo Fisher Scientific Orbitrap Velos Pro mass spectrometer were obtained by photodissociation of weakly bound $D_2$ adducts. The resulting linear action spectra reveal well-resolved band patterns that yield structural identifications of the products by comparison with harmonic calculations for candidates. The hybrid instrument also enables high-resolution mass analysis of ions from an external ion source using the Orbitrap analyzer capability of the Velos platform. The latter capability provides a powerful way to monitor photofragments generated in the vibrational spectroscopy part of the instrument, a next-generation adaptation that is currently being pursued at Yale.

## Acknowledgements

# References

1. Wolk, A.B., Leavitt, C.M., Garand, E., Johnson, M.A.: Cryogenic ion chemistry and spectroscopy. Acc. Chem. Res. **47**, 202–210 (2014)
2. Kamrath, M.Z., Rizzo, T.R.: Combining ion mobility and cryogenic spectroscopy for structural and analytical studies of biomolecular ions. Acc. Chem. Res. **51**, 1487–1495 (2018)
3. Rizzo, T.R., Boyarkin, O.V.: Cryogenic methods for the spectroscopy of large, biomolecular ions. Gas-Phase Ir Spectroscopy and Structure of Biological Molecules Top. Curr. Chem, **364**, 43-98 (2015)
4. Rizzo, T.R., Stearns, J.A., Boyarkin, O.V., et al.: Int. Rev. Phys. Chem. **28**, 481–515 (2009)
5. Boyarkin, O.V.: Cold ion spectroscopy for structural identifications of biomolecules. Int. Rev. Phys. Chem. **37**, 559–606 (2018)
6. Polfer, N.C., Paizs, B., Snoek, L.C., Compagnon, I., Suhai, S., Meijer, G., et al.: Infrared fingerprint spectroscopy and theoretical studies of potassium ion tagged amino acids and peptides in the gas phase. J. Am. Chem. Soc. **123**, 8571 (2005)
7. Roithová, J., Gray, A., Andris, E., Jašík, J., Gerlich, D.: Helium tagging infrared photodissociation spectroscopy of reactive ions. Acc. Chem. Res. **49**, 223–230 (2016)
8. Li, J.-W., Morita, M., Takahashi, K., Kuo, J.-L.: Features in vibrational spectra induced by Ar-tagging for $H_3O^+Ar_m$, m = 0–3. J. Phys. Chem. A. **119**, 10887–10892 (2015)
9. Brummer, M., Kaposta, C., Santambrogio, G., Asmis, K.R.: Formation and photodepletion of cluster ion-messenger atom complexes in a cold ion trap: infrared spectroscopy of $VO^+$, $VO_2^+$, and $VO_3$. J. Chem. Phys. **119**, 12700–12703 (2003)
10. Duong, C.H., Yang, N., Kelleher, P.J., Johnson, M.A., DiRisio, R.J., McCoy, A.B., et al.: Tag-free and isotopomer-selective vibrational spectroscopy of the cryogenically cooled $H_9O_4^+$ cation with two-color, IR-IR double-resonance photoexcitation: isolating the spectral signature of a single OH group in the hydronium ion core. J. Phys. Chem. A. **122**, 9275–9284 (2018)
11. Yang, N., Duong, C.H., Kelleher, P.J., Johnson, M.A., McCoy, A.B.: Isolation of site-specific anharmonicities of individual water molecules in the $I^-·(H_2O)_2$ complex using tag-free, Isotopomer Selective IR-IR Double Resonance. Chem. Phys. Lett. **690**, 159–171 (2017)
12. Heine, N., Yacovitch, T.I., Schubert, F., Brieger, C., Neumark, D.M., Asmis, K.R.: Infrared photodissociation spectroscopy of microhydrated nitrate-nitric acid clusters $NO_3^-(HNO_3)_m(H_2O)_n$. J. Phys. Chem. A. **118**, 7613–7622 (2014)
13. Nagornova, N.S., Rizzo, T.R., Boyarkin, O.V.: Interplay of intra- and intermolecular H-bonding in a progressively solvated macrocyclic peptide. Science. **336**, 320–323 (2012)
14. Chakrabarty, S., Holz, M., Campbell, E.K., Banerjee, A., Gerlich, D., Maier, J.P.: A novel method to measure electronic spectra of cold molecular ions. J. Phys. Chem. Lett. **4**, 4051–4054 (2013)
15. Schmies, M., Patzer, A., Schutz, M., Miyazaki, M., Fujii, M., Dopfer, O.: Microsolvation of the acetanilide cation ($AA^+$) in a nonpolar solvent: IR spectra of $AA^+$-$L_n$ clusters (L = He, Ar, $N_2$; n <= 10). Phys. Chem. Chem. Phys. **16**, 7980–7995 (2014)
16. Liu, H.T., Ning, C.G., Huang, D.L., Wang, L.S.: Vibrational spectroscopy of the dehydrogenated uracil radical by autodetachment of dipole-bound excited states of cold anions. Angew. Chem. Int. Edit. **53**, 2464–2468 (2014)
17. Wolke, C.T., Fournier, J.A., Dzugan, L.C., Fagiani, M.R., Odbadrakh, T.T., Knorke, H., et al.: Spectroscopic snapshots of the proton-transfer mechanism in water. Science. **354**, 1131–1135 (2016)
18. Duffy, E.M., Voss, J.M., Garand, E.: Vibrational characterization of microsolvated electrocatalytic water oxidation intermediate: $[Ru(tpy)(bpy)(OH)]^{2+}(H_2O)_{0-4}$. J. Phys. Chem. A. **121**, 5468–5474 (2017)
19. Redwine, J.G., Davis, Z.A., Burke, N.L., Oglesbee, R.A., McLuckey, S.A., Zwier, T.S.: A novel ion trap based tandem mass spectrometer for the spectroscopic study of cold gas phase polyatomic ions. Int. J. Mass Spectrom. **348**, 9–14 (2013)

20. Feraud, G., Dedonder, C., Jouvet, C., Inokuchi, Y., Haino, T., Sekiya, R., et al.: Development of ultraviolet-ultraviolet hole-burning spectroscopy for cold gas-phase ions. J. Phys. Chem. Lett. **5**, 1236–1240 (2014)

21. Svendsen, A., Lorenz, U.J., Boyarkin, O.V., Rizzo, T.R.: A new tandem mass spectrometer for photofragment spectroscopy of cold, Gas-Phase Molecular Ions. Rev. Sci. Instrum. **81**, 073107 (2010)

22. Heine, N., Asmis, K.R.: Cryogenic ion trap vibrational spectroscopy of hydrogen-bonded clusters relevant to atmospheric chemistry. Int. Rev. Phys. Chem. **34**, 1–34 (2015)

23. Kamrath, M.Z., Garand, E., Jordan, P.A., Leavitt, C.M., Wolk, A.B., Van Stipdonk, M.J., et al.: Vibrational characterization of simple peptides using cryogenic infrared photodissociation of $H_2$-tagged, Mass-Selected Ions. J. Am. Chem. Soc. **133**, 6440–6448 (2011)

24. Marsh, B.M., Voss, J.M., Garand, E.: A dual cryogenic ion trap spectrometer for the formation and characterization of solvated ionic clusters. J. Chem. Phys. **143**, 204201 (2015)

25. Kopysov, V., Makarov, A., Boyarkin, O.V.: Colors for molecular masses: fusion of spectroscopy and mass spectrometry for identification of biomolecules. Anal. Chem. **87**, 4607–4611 (2015)

26. Poltash, M.L., McCabe, J.W., Shirzadeh, M., Laganowsky, A., Clowers, B.H., Russell, D.H.: Fourier transform-ion mobility-Orbitrap mass spectrometer: a next-generation instrument for native mass spectrometry. Anal. Chem. **90**, 10472–10478 (2018)

27. Reinhard, B.M., Lagutschenkov, A., Lemaire, J., Maitre, P., Boissel, P., Niedner-Schatteburg, G.: Reductive nitrile coupling in niobium-acetonitrile complexes probed by free electron laser IR multiphoton dissociation spectroscopy. J. Phys. Chem. A. **108**, 3350–3355 (2004)

28. James, P.: Protein identification in the post-genome era: the rapid rise of proteomics. Q. Rev. Biophys. **30**, 279–331 (1997)

29. Roepstorff, P., Fohlman, J.: Proposal for a common nomenclature for sequence ions in mass-spectra of peptides. Biomed. Mass Spectrom. **11**, 601–601 (1984)

30. Dettmer, K., Aronov, P.A., Hammock, B.D.: Mass spectrometry-based metabolomics. Mass Spectrom. Rev. **26**, 51–78 (2007)

31. Martens, J., Grzetic, J., Berden, G., Oomens, J.: Structural identification of electron transfer dissociation products in mass spectrometry using infrared ion spectroscopy. Nat. Commun. **7**, 11754 (2016)

32. Polfer, N.C., Oomens, J., Suhai, S., Paizs, B.: Infrared spectroscopy and theoretical studies on gas-phase protonated Leu-enkephalin and its fragments: direct experimental evidence for the mobile proton. J. Am. Chem. Soc. **129**, 5887–5897 (2007)

33. Bythell, B.J., Dain, R.P., Curtice, S.S., Oomens, J., Steill, J.D., Groenewold, G.S., et al.: Structure of $[M+H-H_2O]^+$ from protonated tetraglycine revealed by tandem mass spectrometry and IRMPD spectroscopy. J. Phys. Chem. A. **114**, 5076–5082 (2010)

34. Pittman, J.L., O'Connor, P.B.: A minimum thickness gate valve with integrated ion optics for mass spectrometry. J. Am. Soc. Mass Spectrom. **16**, 441–445 (2005)

35. Frisch, M.J., Trucks, G.W., Schlegel, H.B., Scuseria, G.E., Robb, M.A., Cheeseman, J.R., et al.: Gaussian 09, Revision D.01. (2009)

36. Stearns, J.A., Mercier, S., Seaiby, C., Guidi, M., Boyarkin, O.V., Rizzo, T.R.: Conformation-specific spectroscopy and photodissociation of cold, protonated tyrosine and phenylalanine. J. Am. Chem. Soc. **129**, 11814–11820 (2007)

37. Masellis, C., Khanal, N., Kamrath, M.Z., Clemmer, D.E., Rizzo, T.R.: Cryogenic vibrational spectroscopy provides unique fingerprints for glycan identification. J. Am. Soc. Mass Spectrom. **28**, 2217–2222 (2017)

38. Mucha, E., González Flórez, A.I., Marianski, M., Thomas, D.A., Hoffmann, W., Struwe, W.B., et al.: Glycan fingerprinting via cold-ion infrared spectroscopy. Angew. Chem. Int. Ed. **56**, 11248–11251 (2017)

39. Lioe, H., O'Hair, R.A.J.: Comparison of collision-induced dissociation and electron-induced dissociation of singly protonated aromatic amino acids, cystine and related simple peptides using a hybrid linear ion trap-FT-ICR mass spectrometer. Anal. Bioanal. Chem. **389**, 1429–1437 (2007)

40. Scott, N.E., Parker, B.L., Connolly, A.M., Paulech, J., Edwards, A.V.G., Crossett, B., et al.: Simultaneous glycan-peptide characterization using hydrophilic interaction chromatography and parallel fragmentation by CID, higher energy collisional dissociation, and electron transfer dissociation MS applied to the N-linked glycoproteome of campylobacter jejuni. Mol. Cell. Proteomics. **10**, M000031–MMCP201 (2011)

41. Falick, A.M., Hines, W.M., Medzihradszky, K.F., Baldwin, M.A., Gibson, B.W.: Low-mass ions produced from peptides by high-energy collision-induced dissociation in tandem mass-spectrometry. J. Am. Soc. Mass Spectrom. **4**, 882–893 (1993)

42. Dass, C.: Fundamentals of contemporary mass spectrometry. John Wiley & Sons (2007)